

# Thermal and Nonlinear Dissipative-Soliton Dynamics in Kerr Microresonator Frequency Combs

Jordan R. Stone,<sup>1,2</sup> Travis C. Briles,<sup>1,2</sup> Tara E. Drake,<sup>1</sup> Daryl T. Spencer,<sup>1</sup> David R. Carlson,<sup>1</sup> Scott A. Diddams,<sup>1,2</sup> and Scott B. Papp<sup>1,2</sup>

<sup>1</sup>*Time and Frequency Division, National Institute for Standards and Technology, Boulder, CO 80305\**

<sup>2</sup>*Department of Physics, University of Colorado Boulder, Boulder, CO 80309*

(Dated: September 6, 2022)

We report on radiofrequency techniques to generate and control dissipative-Kerr-soliton microresonator frequency combs on demand. Since the relative detuning of the pump laser and resonator primarily determines soliton dynamics, we devise an offset Pound-Drever-Hall (PDH) frequency-locking system to directly control and stabilize the detuning with radiofrequency precision. PDH locking not only guides Kerr-soliton formation from a cold resonator, but it enables systematic exploration of the detuning-dependent thermal and nonlinear processes that govern the frequency comb and opens a path to decouple its repetition and carrier-envelope-offset frequencies. In particular, we demonstrate phase stabilization of both these degrees-of-freedom with a single-soliton Kerr comb to a fractional frequency precision below  $10^{-16}$ , to be compatible with optical-timekeeping technology. Moreover, we investigate the fundamental role that residual detuning noise plays in the spectral purity of Kerr-comb microwave generation.

Kerr solitons in optical microresonators provide a unique platform for compact, low-noise, microwave-rate, and low-power frequency-comb generation [1, 2]. To date, soliton microresonator frequency combs have been used to demonstrate several fundamental nonlinear photonics concepts, from soliton crystallization to dark-soliton formation [3–5], and micro-scale technologies, including optical clocks [6], optical frequency synthesis [7], communications [8–10], sensing [11, 12], and low-noise microwave oscillators [13]. One central challenge cutting across these directions is the reliable generation of dissipative-Kerr solitons, which are pulses of light balancing nonlinearity, dispersion, gain, and loss. They are parameterized by the relative detuning of the pump laser and Kerr microresonator, and respond to fluctuations in the intracavity field in only a few photon lifetimes; as a result, detuning control is critical [14–19].

Technical issues like bistability [20] also impact microresonators and Kerr-soliton formation, and microresonator mode imperfections introduce intracavity noise even within a single roundtrip, suppressing soliton formation [21]. Moreover, a fundamental efficiency of Kerr solitons, especially at microwave-rate repetition frequencies, is a high quality factor ( $Q$ ) to enable milliwatt threshold power [22, 23], but this necessitates operation of the pump laser within a narrow, red-detuned frequency window near resonance. Practical experiments utilize servo control to overcome these issues and maintain soliton operation [19, 24], but this interferes with independent control of the carrier-envelope-offset ( $f_{\text{ceo}}$ ) [25] and repetition ( $f_{\text{rep}}$ ) frequencies central to frequency-comb applications. Previous microcomb locking experiments have leveraged either blue-detuned combs [26], multiple-soliton states [6, 27] or lower  $Q$  resonators in which laser tunability is unrestricted [28, 29].

In this Letter, we report on a general mechanism to

initiate single (or higher number) Kerr solitons from a cold resonator that results in stable radiofrequency (RF) control of the pump detuning, and in turn of the soliton dynamics and the frequency comb's  $f_{\text{ceo}}$  and  $f_{\text{rep}}$ . We show how a single-sideband, suppressed-carrier (SSB-SC) optical-frequency shifter provides agile scanning much faster than the thermal bistability and evolution of the intracavity field. Moreover, Pound-Drever-Hall (PDH) spectroscopy [30] identifies the Kerr resonance with high signal-to-noise ratio, and an RF offset we apply through the PDH system enables stable detuning control. By rapidly scanning the pump laser from blue-to-red detuning, we observe formation of a chaotic Kerr comb and the transition to a soliton Kerr comb; we stabilize the pump laser to the resonance as the soliton waveform settles. PDH locking gives unprecedented control over the pump-resonator detuning  $\delta$ , which we use to decouple  $f_{\text{ceo}}$  and  $f_{\text{rep}}$  for their straightforward phase stabilization, and to explore low-noise photonic-microwave generation.

We perform the experiments with a 22 GHz free-spectral range (FSR) silica wedge resonator sample that has quality factor of 180 million [24]. The resonator is fabricated on a silicon substrate, and light is coupled to the device via a tapered fiber. Figure 1(a) presents the experimental setup. The output from an external-cavity diode laser (ECDL) is sent through an SSB-SC frequency shifter composed of a dual-parallel lithium niobate waveguide Mach-Zehnder intensity modulator [31] driven by a wideband voltage-controlled oscillator (VCO); we have measured frequency-scan rates up to 100 GHz/ $\mu\text{s}$  with 4 GHz range. We derive the PDH error signal by applying RF phase-modulation sidebands to the pump laser before it enters the silica resonator and photodetect them after the resonator. Operationally, the lock point of the PDH servo corresponds to the higher frequency PDH sideband on resonance and the pump laser

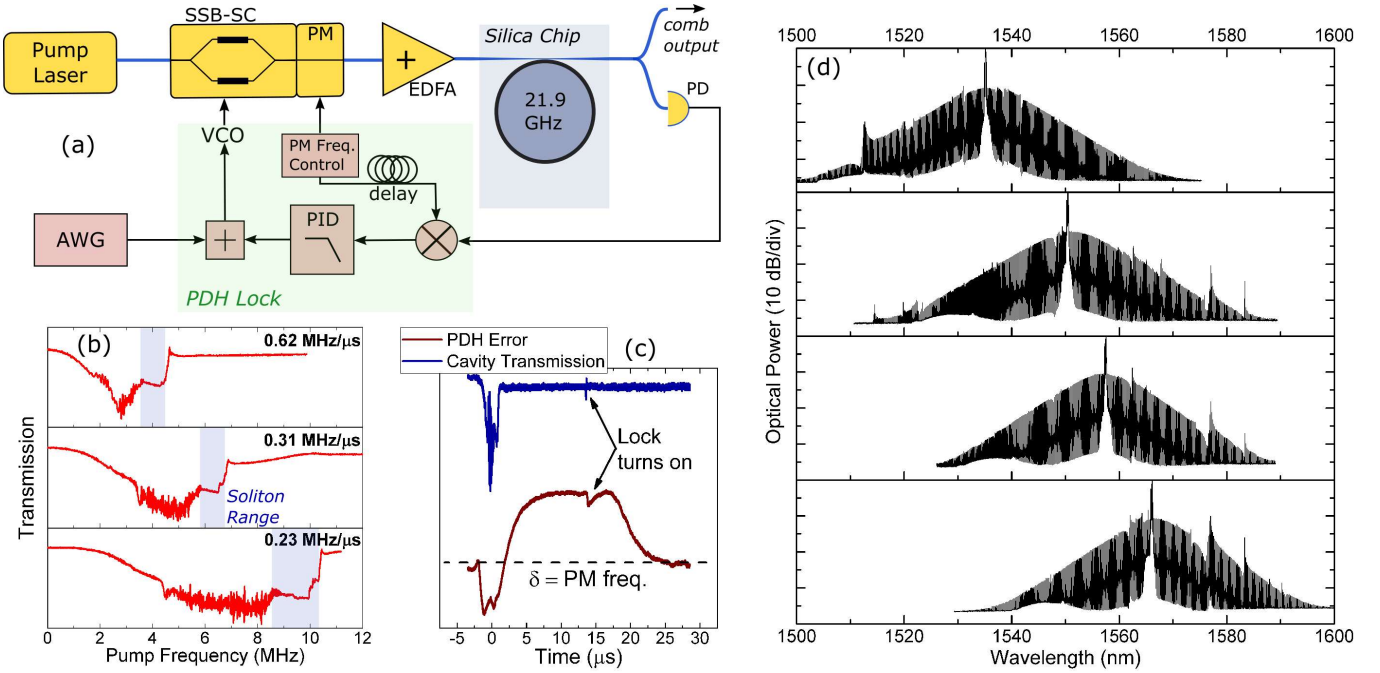


FIG. 1. (a) PDH scheme for Kerr-soliton generation. An SSB-SC frequency shifter is driven by a high-bandwidth VCO for fast frequency control of the pump laser, and a servo locks one of the phase-modulation (PM) sidebands at resonance. (b) By adjusting the pump frequency sweep rate, we optimize the transition to Kerr solitons from a cold resonator. The waveform applied to the VCO is a simple, linear voltage sweep. (c) Feedback is initiated at a pre-determined instant of the frequency scan. (d) Generation of soliton frequency combs across the entire C-Band.

red-detuned by the phase-modulation frequency [32, 33]. While we can widely adjust the frequency scan rate to controllably generate Kerr solitons [Fig. 1(b)], we optimize so that solitons form in thermal equilibrium [1]; see Fig. 1(c). Importantly, we obtain single-Kerr-soliton states across the entire C-band range of the diode laser, as shown in Fig. 1(d), even as resonator mode-family degeneracies contribute 10 dB excursions to the soliton spectrum.

Building on robust acquisition of single Kerr solitons, we explore their frequency stabilization with respect to an optical reference. This goal, or stabilization through the  $f - 2f$  technique [34], requires simultaneous control over both  $f_{\text{rep}}$  and  $f_{\text{ceo}}$ , which define the comb-line frequencies through the well-known relation

$$\nu_m = f_{\text{ceo}} + m \times f_{\text{rep}}, \quad (1)$$

where  $\nu_m$  is the frequency of each comb mode, indexed by the integer  $m$  [25]. In operation,  $f_{\text{ceo}}$  and  $f_{\text{rep}}$  of a Kerr comb are coupled via nonlinear and thermal effects, which depend on both the pump power and  $\delta$  – the independent variables in our experiment. For example, the repetition frequency of a soliton Kerr comb is approximated by

$$2\pi f_{\text{rep}} = D_1 + \Omega D_2/D_1, \quad (2)$$

where  $D_1$  and  $D_2$  are the first- and second-order dispersions [35], and  $\Omega$  is the soliton self-frequency shift

(SSFS) that results from a combination of Raman and mode-perturbation effects [36]. The SSFS describes a frequency shift in the comb spectrum relative to the pump frequency, and is therefore coupled to the repetition rate through second-order dispersion. Moreover, the SSFS is directly proportional to  $\delta$  [36]; thus the detuning controls  $f_{\text{rep}}$  through the SSFS, while the pump power thermo-optically tunes  $f_{\text{rep}}$  through  $D_1$ . At the same time, an exact relationship exists between  $f_{\text{ceo}}$ , the pump-laser frequency  $\nu_p$ , and  $f_{\text{rep}}$ , namely

$$f_{\text{ceo}} = \nu_p - N \times f_{\text{rep}}, \quad (3)$$

where  $N$  counts the positive integer number of comb modes such that  $N \times f_{\text{rep}} \approx \nu_p$ . Clearly, simultaneous stabilization of  $\nu_p$  and  $f_{\text{rep}}$  implies the stability of  $f_{\text{ceo}}$ , which is the relevant parameter for users of the comb who likely do not require (or desire) knowledge of the Kerr-comb dynamics internal to the microresonator. Therefore,  $\nu_p$  must be adjusted to serve two purposes at the same time: (1) Maintain  $\delta$  within the appropriate range for stable Kerr-soliton propagation and (2) Be phase-locked or tuned subject to user requirements.

Satisfying the above criteria while maintaining independent control over  $f_{\text{rep}}$  necessitates the decoupling of the frequency-comb degrees-of-freedom. We therefore search for settings of pump power and detuning that allow  $f_{\text{rep}}$  to be adjusted without disturbing  $\nu_p$ . This leads us to study the coupled dynamics of  $\nu_p$  and  $f_{\text{rep}}$

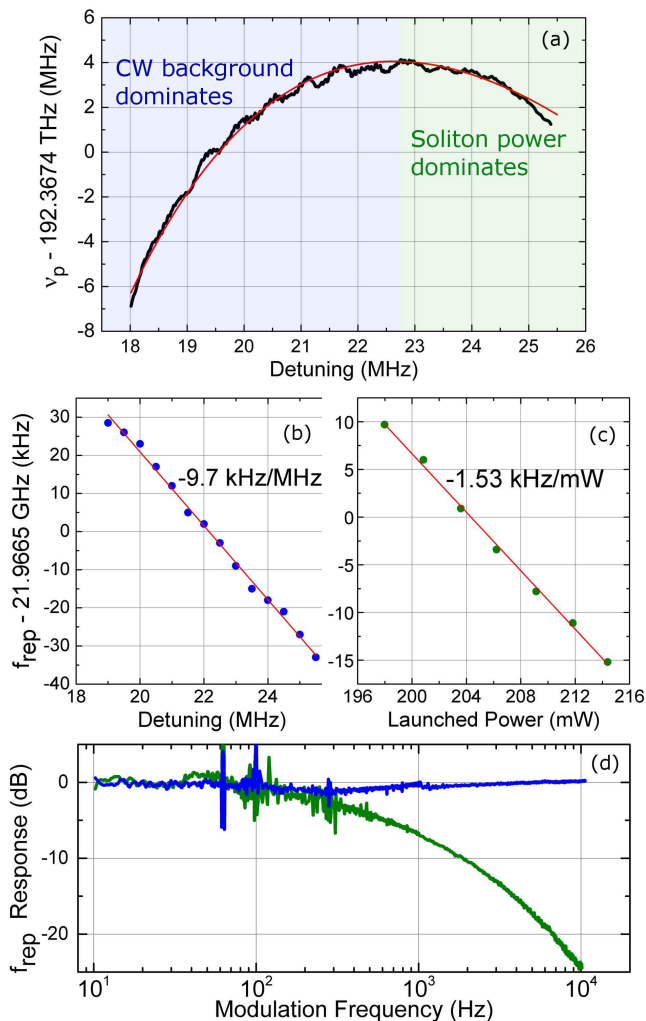


FIG. 2. (a) The CW power and soliton power balance to determine the dependence of pump frequency on detuning. The red curve is the integral of Eq. (4) scaled by the cavity frequency rate-of-change with intracavity power. (b) Dependence of soliton repetition frequency with detuning. (c) Dependence of soliton repetition frequency with pump power. Red lines in (b,c) are linear fits. (d) Soliton repetition-frequency response to detuning (blue) and pump-power (green).

and, specifically, their dependence on pump power and detuning (Fig. 2). Note that, in our experiments,  $\nu_p$  is PDH-servo-controlled to maintain a particular value of  $\delta$ . Therefore the thermo-optic effect [20] couples  $\nu_p$  to the intracavity power ( $P_{cav}$ ), which is the sum of a CW background associated with the pump laser [1] and the soliton pulse. For a single Kerr soliton and  $\delta \gg \Gamma$  ( $\Gamma$  is the resonator linewidth), the rate-of-change of  $P_{cav}$  with  $\delta$  is [1, 24]

$$\frac{\partial P_{cav}}{\partial \delta} = \frac{\eta n A_{eff}}{n_2 Q D_1} \sqrt{\frac{2D_2}{\delta}} - 2\Gamma^2 F^2 / \delta^3, \quad (4)$$

where  $A_{eff}$  is the effective mode area,  $\eta$  is the coupling efficiency,  $n$  is the refractive index,  $n_2$  is the nonlinear

refractive index, and  $F^2$  is the pump power normalized to the comb threshold power. According to Eq. (4), the soliton pulse and CW background [the first and second terms on the right side of Eq. (4), respectively] compete to determine the sign of  $\partial P_{cav}/\partial \delta$ , and which term dominates depends on the magnitude of  $\delta$ . While the CW background primarily determines  $\partial P_{cav}/\partial \delta$  at small red  $\delta$ , it becomes negligible at larger red  $\delta$ , and Eq. (4) may be approximated using only the soliton term. Hence, we find that Kerr-soliton frequency combs operate in essentially two  $\delta$  regimes: (1)  $\partial P_{cav}/\partial \delta < 0$  and  $\nu_p$  tunes opposite to  $\delta$ , (2)  $\partial P_{cav}/\partial \delta > 0$  and  $\nu_p$  tunes with the same sign as  $\delta$ . At the crossover of these two regimes a “fixed point” of the frequency comb [37] exists.

To test our understanding of these dynamics, we vary  $\delta$  through the PDH lock and record on an oscilloscope the PDH servo output that controls the VCO. Multiplying by the VCO tuning coefficient (Hz/V) determines  $\nu_p$  during the sweep [Fig. 2(a)]. For comparison, we integrate Eq. (4) to generate a prediction curve for Fig. 2(a). Equation (4) accurately predicts the  $\nu_p$  behavior in both the blue-shaded region, where the pump dynamics are largely determined by the CW background, and the green region, where the soliton physics dominates. In particular, the model identifies the turning point between 22 MHz and 23 MHz. Additionally, we record in Fig. 2(b,c) the dependence of  $f_{rep}$  on both  $\delta$  and pump power. Evidently, either of these may be used to tune the repetition frequency; however, they provide different sensitivities. Because the pump power relies on thermal effects to control  $f_{rep}$ , the response bandwidth is limited by the resonator thermal response time [20], whereas control of  $f_{rep}$  through  $\delta$  is limited by the SSFS response and practically limited by the bandwidth of the PDH lock [see Fig. 2(d)] [38].

In view of the results shown in Fig. 2, an optimal strategy is to decouple the  $f_{rep}$  and  $f_{ceo}$  frequencies of the comb by operating about the detuning that corresponds to a  $\nu_p$  fixed point. Figure 3 presents a detailed schematic and measurement results that demonstrate this strategy. We tune  $f_{rep}$  through feedback to  $\delta$  (by modulating the PDH frequency) and phase-lock it to a hydrogen-maser-referenced  $\sim 22$  GHz oscillator. We directly phase-lock  $\nu_p$  to an ultralow-expansion glass Fabry-Perot (FP) stabilized laser at 1550 nm, using the Kerr comb’s pump power. To characterize the residual noise in our optical and microwave phase-locks, we form an electro-optic (EO) frequency comb around the FP-stabilized laser, using a microwave oscillator synthesized from the same H-maser reference; see Fig. 3(a). By measuring the frequency noise of optical-heterodyne beatnotes between the Kerr and EO combs, we characterize the residual frequency-noise contributions from our two phase locks and the microwave noise contribution of the EO comb. Our Allan deviation measurements [Fig. 3(c)] of the optical heterodyne signals quantify this residual noise [39].

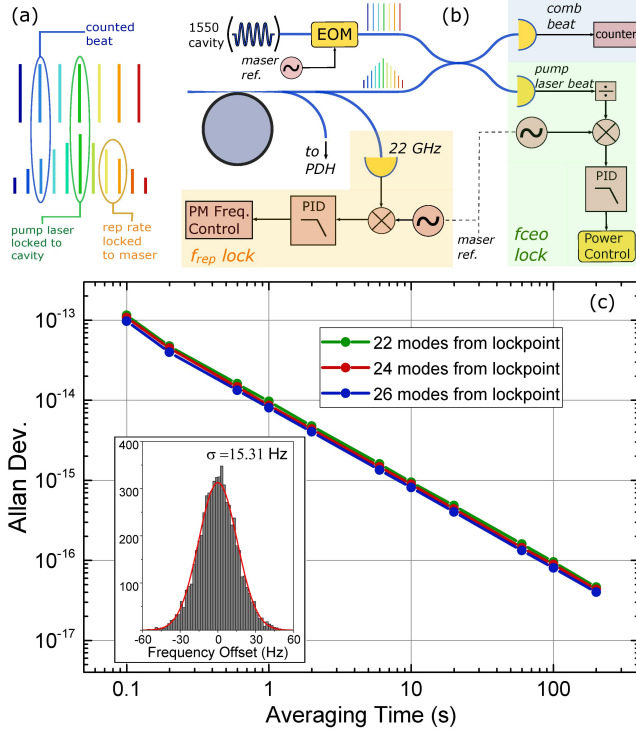


FIG. 3. (a) Illustration of the experiment to characterize residual noise in our phase locks of  $f_{\text{rep}}$  and  $f_{\text{ceo}}$ . The pump laser is phase-locked to a cavity-stabilized laser, which is electro-optically (EO) modulated to produce a reference comb. The repetition rates of both combs are derived from the same reference. (b) Setup used to fully stabilize the Kerr comb. (c) Allan deviations of three Kerr comb lines counted against neighboring EO teeth. Inset: Distribution of counted frequencies at 0.1 s gate time with a Gaussian fit (red line). The error between the mean and the expected value is 2 mHz.

The performance of our Kerr-comb system, with its ability to perform frequency metrology with  $10^{-16}$  imprecision, is commensurate with modern optical-timekeeping technology. Moreover, the inaccuracy of our phase-locked Kerr-comb, which we also assess from the EO-comb heterodyne signals, is less than 5 mHz for all data sets and consistent with the Allan deviation at all values of averaging time.

Photonic microwave-signal generation is an important application of frequency combs [40]. We explore the relative intensity noise (RIN) of our Kerr comb and the single-sided, single-sideband phase noise ( $L_\phi(f)$ ) of its 21.98 GHz microwave repetition frequency under the novel conditions enabled by our PDH detuning lock; the black traces in Fig. 4(a,b) present our measurements. Since  $L_\phi(f)$  is lower than that of many commercial microwave synthesizers, we use a self-referenced EO frequency comb operated as an optical-frequency divider to provide a reference oscillator at 22 GHz [41]. Prior to photodetecting  $f_{\text{rep}}$ , we bandstop filter residual pump light, and re-amplify the remaining soliton comb to  $\sim 10$  mW. Both the RIN and  $L_\phi(f)$  exhibit typical technical-

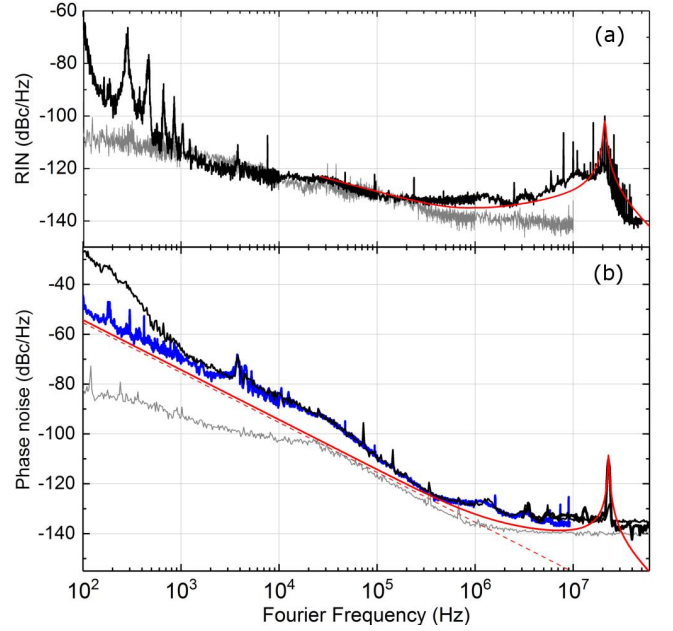


FIG. 4. (a) Relative intensity noise (RIN, black and gray traces) of the Kerr comb and pump laser, and model prediction (red trace) as described in the text. (b) Measured phase noise of  $f_{\text{rep}}$  (black traces), and predictions obtained from our model (red) and the PDH error signal (blue), respectively. The gray trace is the measurement-system floor. The red dashed line indicates our phase-noise prediction in the absence of resonant noise conversion.

driven fluctuations at Fourier frequencies  $\lesssim 10$  kHz. Here we focus on the Kerr-comb noise floor beyond 10 kHz, which has been of significant interest but for which a complete explanation has not yet emerged [13, 42]. At the highest Fourier frequency range of our measurements, the  $-135$  dBc/Hz phase noise we obtain is significantly above the shot-noise contribution of the photodetected comb light, and any white-frequency-noise mechanism that affects the soliton pulse circulating in the microresonator would not result in such a frequency-independent noise floor. Moreover, the Kerr-comb RIN significantly exceeds the shot-noise-limited pump-laser RIN [38]. Understanding this issue is important for future applications.

Based on an analysis of  $\nu_p$ -to- $f_{\text{rep}}$  noise conversion and on the characterization presented earlier in Fig. 2, we model the contributions to  $L_\phi(f)$ . First, we assess that for single Kerr solitons circulating in a high- $Q$  microresonator, detuning noise is the most important contribution. With  $\delta \gg \Gamma$ , the typical white-frequency-noise spectrum of an ECDL leads to enhanced peaks at  $f = \delta$  in the RIN and  $L_\phi(f)$  spectra. Specifically, we predict that

$$L_\phi(f) = \frac{\partial f_{\text{rep}}}{\partial \delta} \frac{1}{f^2} \left( \frac{\nu_c n_2}{n A_{\text{eff}}} \right)^2 S_{I,\text{cav}}(f), \quad (5)$$

where  $\partial f_{\text{rep}}/\partial \delta$  is the conversion factor of  $\delta$  noise to  $f_{\text{rep}}$  frequency noise,  $S_{I,\text{cav}}(f)$  is the intracavity inten-

sity noise calculated for a white-frequency-noise pump laser [43], and  $\nu_c$  is the microresonator frequency. The red trace in Fig. 4(b) shows how this model mostly captures our measured  $L_\phi(f)$  noise floor, particularly the enhancement at the Fourier frequency corresponding to the  $\delta = 23$  MHz setting used here, while the red trace in Fig. 4(a) shows the related comb RIN within our model. Separately, we infer  $L_\phi(f)$  from the PDH error signal, which indicates the remaining  $\delta$  noise affecting Kerr soliton propagation, accounting for the  $f_{\text{rep}}$  response given in Fig. 2(d). In Fig. 4(b), the blue trace is this result, which reproduces our  $L_\phi(f)$  measurement well due to the wide bandwidth, high SNR available, and straightforward calibration of the PDH error signal. We anticipate that improved photonic microwave generation would be possible should we incorporate a lower noise laser into our system. In this case, a still lower noise reference oscillator would be required for phase-noise metrology, or more precise techniques such as cross correlation might be useful, depending on the impact of Kerr-comb RIN.

In summary, we have introduced a novel system for generating and controlling dissipative Kerr solitons in microresonators. We already utilize the technique with multiple microresonator platforms [29, 44], including in SiN resonators that had previously required a specific dispersion profile to balance the thermal bistability and mode-perturbation effects [17]. Rapid frequency scanning and PDH locking could be implemented with discrete semiconductor lasers and Kerr microresonators, or potentially in a heterogeneously integrated Kerr-comb platform. Moreover, our techniques and analysis may be used in numerous frequency-comb applications, including spectroscopy, low-noise microwave generation, optical frequency synthesis, and optical clocks.

We thank X. Yi, K. Yang, and K. Vahala at Caltech for assisting and for fabricating the resonator used in the experiment, as well as L. Stern and Z. Newman for valuable thoughts on the manuscript. This project was funded by NIST and the DARPA DODOS program. This work is a contribution of the U.S. government and is not subject to copyright.

---

\* jordan.stone@colorado.edu

- [1] T. Herr, V. Brasch, J. Jost, C. Wang, N. Kondratiev, M. Gorodetsky, and T. Kippenberg, *Nature Photonics* **8**, 145 (2014).
- [2] S. Coen, H. G. Randle, T. Sylvestre, and M. Erkintalo, *Optics letters* **38**, 37 (2013).
- [3] D. C. Cole, E. S. Lamb, P. Del’Haye, S. A. Diddams, and S. B. Papp, arXiv preprint arXiv:1610.00080 (2016).
- [4] X. Xue, Y. Xuan, Y. Liu, P.-H. Wang, S. Chen, J. Wang, D. E. Leaird, M. Qi, and A. M. Weiner, *Nature Photonics* **9**, 594 (2015).
- [5] K. Y. Y. Qi-Fan Yang, Xu Yi and K. Vahala, *Nature Physics* **13**, 53 (2016).
- [6] S. B. Papp, K. Beha, P. Del’Haye, F. Quinlan, H. Lee, K. J. Vahala, and S. A. Diddams, *Optica* **1**, 10 (2014).
- [7] D. Spencer *et al.*, arXiv preprint arXiv:1708.05228 (2017).
- [8] J. Pfeifle, V. Brasch, M. Lauer, Y. Yu, D. Wegner, T. Herr, K. Hartinger, P. Schindler, J. Li, D. Hillerkuss, *et al.*, *Nature photonics* **8**, 375 (2014).
- [9] F. Leo, S. Coen, P. Kockaert, S.-P. Gorza, P. Emplit, and M. Haelterman, *Nature Photonics* **4**, 471 (2010).
- [10] P. Marin-Palomo, J. N. Kemal, M. Karpov, A. Kordts, J. Pfeifle, M. H. Pfeiffer, P. Trocha, S. Wolf, V. Brasch, R. Rosenberger, *et al.*, *Nature* **546**, 274 (2017).
- [11] M.-G. Suh, Q.-F. Yang, K. Y. Yang, X. Yi, and K. J. Vahala, *Science* **354**, 600 (2016).
- [12] P. Trocha *et al.*, arXiv preprint arXiv:1707.05969.
- [13] W. Liang, D. Eliyahu, V. Ilchenko, A. Savchenkov, A. Matsko, D. Seidel, and L. Maleki, *Nature communications* **6** (2015).
- [14] X. Yi, Q.-F. Yang, K. Y. Yang, and K. Vahala, *Optics letters* **41**, 2037 (2016).
- [15] H. Guo, M. Karpov, E. Lucas, A. Kordts, M. Pfeiffer, V. Brasch, G. Lihachev, V. Lobanov, M. Gorodetsky, and T. Kippenberg, *Nature Physics* (2016).
- [16] C. Joshi, J. K. Jang, K. Luke, X. Ji, S. A. Miller, A. Klenner, Y. Okawachi, M. Lipson, and A. L. Gaeta, *Optics letters* **41**, 2565 (2016).
- [17] Q. Li, T. C. Briles, D. A. Westly, T. E. Drake, J. R. Stone, B. R. Ilic, S. A. Diddams, S. B. Papp, and K. Srinivasan, *Optica* **4**, 193 (2017).
- [18] E. Obrzud, S. Lecomte, and T. Herr, arXiv preprint arXiv:1612.08993 (2016).
- [19] E. Lucas, H. Guo, J. D. Jost, M. Karpov, and T. J. Kippenberg, *Physical Review A* **95**, 043822 (2017).
- [20] T. Carmon, L. Yang, and K. J. Vahala, *Optics Express* **12**, 4742 (2004).
- [21] T. Herr, V. Brasch, J. Jost, I. Mirgorodskiy, G. Lihachev, M. Gorodetsky, and T. Kippenberg, *Physical review letters* **113**, 123901 (2014).
- [22] X. Ji, F. A. Barbosa, S. P. Roberts, A. Dutt, J. Cardenas, Y. Okawachi, A. Bryant, A. L. Gaeta, and M. Lipson, *Optica* **4**, 619 (2017).
- [23] H. Lee, T. Chen, J. Li, K. Y. Yang, S. Jeon, O. Painter, and K. J. Vahala, *Nature Photonics* **6**, 369 (2012).
- [24] X. Yi, Q.-F. Yang, K. Y. Yang, M.-G. Suh, and K. Vahala, *Optica* **2**, 1078 (2015).
- [25] D. J. Jones, S. A. Diddams, J. K. Ranka, A. Stentz, R. S. Windeler, J. L. Hall, and S. T. Cundiff, *Science* **288**, 635 (2000).
- [26] P. Del’Haye, O. Arcizet, A. Schliesser, R. Holzwarth, and T. J. Kippenberg, *Physical Review Letters* **101**, 053903 (2008).
- [27] P. Del’Haye, A. Coillet, T. Fortier, K. Beha, D. C. Cole, K. Y. Yang, H. Lee, K. J. Vahala, S. B. Papp, and S. A. Diddams, *Nature Photonics* **10**, 516 (2016).
- [28] V. Brasch, E. Lucas, J. D. Jost, M. Geiselmann, and T. J. Kippenberg, *Light: Science and Applications* **6** (2017).
- [29] T. C. Briles, T. Drake, D. Spencer, J. R. Stone, C. Fredrick, Q. Li, D. Westly, B. Ilic, X. Yi, K. Y. Yang, *et al.*, in *CLEO: Science and Innovations* (Optical Society of America, 2017) pp. SW4N-3.
- [30] R. Drever, J. L. Hall, F. Kowalski, J. Hough, G. Ford, A. Munley, and H. Ward, *Applied physics B: Lasers and optics* **31**, 97 (1983).

- [31] J. Wang, D. Chen, H. Cai, F. Wei, and R. Qu, *Optics express* **23**, 7038 (2015).
- [32] J. I. Thorpe, K. Numata, and J. Livas, *Optics express* **16**, 15980 (2008).
- [33] D. Gatti, R. Gotti, T. Sala, N. Coluccelli, M. Belmonte, M. Prevedelli, P. Laporta, and M. Marangoni, *Optics letters* **40**, 5176 (2015).
- [34] S. A. Diddams, D. J. Jones, J. Ye, S. T. Cundiff, J. L. Hall, J. K. Ranka, R. S. Windeler, R. Holzwarth, T. Udem, and T. Hänsch, *Physical Review Letters* **84**, 5102 (2000).
- [35] T. Herr, K. Hartinger, J. Riemensberger, C. Wang, E. Gavartin, R. Holzwarth, M. Gorodetsky, and T. Kippenberg, *Nature Photonics* **6**, 480 (2012).
- [36] X. Yi, Q.-F. Yang, X. Zhang, K. Y. Yang, X. Li, and K. Vahala, *Nature Communications* **8**, 14869 (2017).
- [37] N. R. Newbury and W. C. Swann, *JOSA B* **24**, 1756 (2007).
- [38] W. Loh, J. Becker, D. C. Cole, A. Coillet, F. N. Baynes, S. B. Papp, and S. A. Diddams, *New Journal of Physics* **18**, 045001 (2016).
- [39] F. Riehle, *Frequency standards: basics and applications* (John Wiley & Sons, 2006).
- [40] T. M. Fortier, M. S. Kirchner, F. Quinlan, J. Taylor, J. Bergquist, T. Rosenband, N. Lemke, A. Ludlow, Y. Jiang, C. Oates, *et al.*, *Nature Photonics* **5**, 425 (2011).
- [41] D. Carlson *et al.*, manuscript in preparation.
- [42] S. B. Papp and S. A. Diddams, *Physical Review A* **84**, 053833 (2011).
- [43] T. J. Kippenberg, A. Schliesser, and M. Gorodetsky, *New Journal of Physics* **15**, 015019 (2013).
- [44] E. S. Lamb, J. R. Stone, M.-G. Suh, K. Vahala, S. Diddams, and S. Papp, in *CLEO: Science and Innovations* (Optical Society of America, 2017) pp. SF1C–4.